



Molecular Crystals and Liquid Crystals Science and Technology. Section A. Molecular Crystals and Liquid Crystals

Publication details, including instructions for authors and
subscription information:

<http://www.tandfonline.com/loi/gmcl19>

Frequency Dependent Conductivity in Organic Superconductors

Martin Dressel^{a, b} & George Grüner^a

^a Department of Physics, University of California, Los Angeles,
CA, 90095, U.S.A.

^b Institut für Festkörperphysik, Technische Hochschule
Darmstadt, Hochschulstr. 6, D-64289, Darmstadt, Germany E-
mail:

Version of record first published: 24 Sep 2006.

To cite this article: Martin Dressel & George Grüner (1996): Frequency Dependent Conductivity in
Organic Superconductors, Molecular Crystals and Liquid Crystals Science and Technology. Section
A. Molecular Crystals and Liquid Crystals, 284:1, 107-119

To link to this article: <http://dx.doi.org/10.1080/10587259608037915>

PLEASE SCROLL DOWN FOR ARTICLE

Full terms and conditions of use: <http://www.tandfonline.com/page/terms-and-conditions>

This article may be used for research, teaching, and private study purposes. Any
substantial or systematic reproduction, redistribution, reselling, loan, sub-licensing,
systematic supply, or distribution in any form to anyone is expressly forbidden.

The publisher does not give any warranty express or implied or make any
representation that the contents will be complete or accurate or up to date. The
accuracy of any instructions, formulae, and drug doses should be independently
verified with primary sources. The publisher shall not be liable for any loss, actions,
claims, proceedings, demand, or costs or damages whatsoever or howsoever caused
arising directly or indirectly in connection with or arising out of the use of this material.

FREQUENCY DEPENDENT CONDUCTIVITY IN ORGANIC SUPERCONDUCTORS

MARTIN DRESSEL¹ and GEORGE GRÜNER

Department of Physics, University of California, Los Angeles, CA 90095, U.S.A.

Abstract Optical studies, in a wide sense, are one of the most powerful techniques for studying the electronic properties of solids. We discuss investigations of the electrodynamic response in the two-dimensional organic conductors of the BEDT-TTF family, which become superconducting at around 10 K. In the normal state, the frequency dependent conductivity is that of a weakly correlated metal with significant deviations from a simple Drude metal. The electro-dynamical properties of the superconducting state are those of an anisotropic, but conventional BCS superconductor.

INTRODUCTION

Since the early and most important studies of $(\text{TMTSF})_2X$ by Jacobsen et al. [1], it is generally acknowledged that optical experiments give valuable information on the electronic properties of organic conductors and superconductors. In the case of the organic superconductor $(\text{BEDT-TTF})_2\text{Cu}(\text{NCS})_2$ and its sister compounds, the experimental results in the optical range of the spectrum [2, 3, 4] and in the microwave range [5, 6, 7, 8] are well established. Combining the findings obtained by different techniques, it is possible to reconsider the complete electrodynamic response. We discuss the optical properties of the BEDT-TTF salts in the normal state as well as in the superconducting ground state.

NORMAL STATE PROPERTIES

The κ -phase of $(\text{BEDT-TTF})_2\text{Cu}(\text{NCS})_2$ is among the most prominent of many charge transfer salts [9]. The BEDT-TTF molecules form conducting sheets in the (bc) -plane separated by polymeric anions $\text{Cu}(\text{NCS})_2^-$. For $(\text{BEDT-TTF})_2\text{Cu}(\text{NCS})_2$, the room temperature conductivity of the highly conducting (bc) -plane is about $20 (\Omega\text{cm})^{-1}$ with an in-plane anisotropy σ_c/σ_b of approximately 2 and an out-of-plane ratio σ_c/σ_a larger than 5000 [10, 11]. Hence the $(\text{BEDT-TTF})_2X$ compounds are called two-dimensional conductors.

We have conducted experiments on the low frequency ($\hbar\omega < \Delta$) electrodynamic response in the normal and superconducting state of $(\text{BEDT-TTF})_2\text{Cu}(\text{NCS})_2$, by measuring the surface impedance \hat{Z}_S at microwave and millimeter wave frequencies (35 GHz up to 100 GHz, i.e. 1 cm^{-1} to 3 cm^{-1}) down to $T = 0.8 \text{ K}$. We employed cylindrical TE_{011} cavities in transmission configuration and measure the cavity parameters (resonance frequency and bandwidth) as a function of temperature. From both quantities the complex surface impedance $\hat{Z}_S(T)$ can be evaluated [12, 13, 14].

¹present address: Institut für Festkörperphysik, Technische Hochschule Darmstadt, Hochschulstr. 6, D-64289 Darmstadt, Germany; internet: di7o@hrzpub.th-darmstadt.de

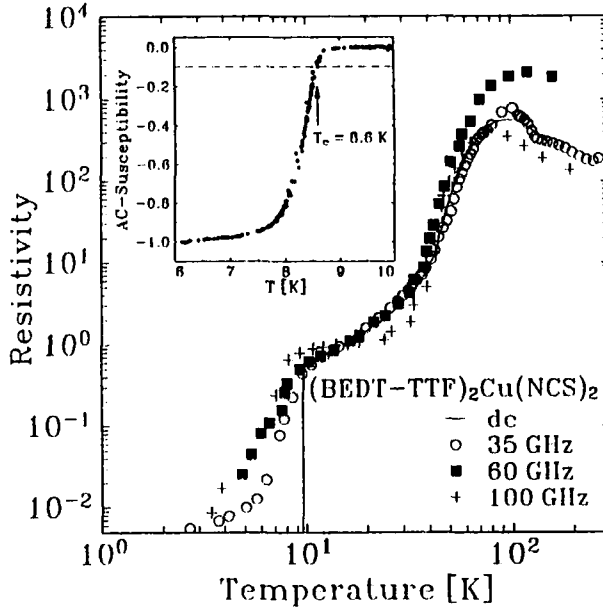


FIGURE 1: The temperature dependence of the in-plane resistivity of $(\text{BEDT-TTF})_2\text{Cu}(\text{NCS})_2$ measured at different frequencies. $R_S^2/\mu_0\omega$ is shown for the microwave and millimeter wave data. The curves are normalized to their 15 K-value. The inset displays a typical magnetization curve of $\kappa\text{-(BEDT-TTF)}_2\text{Cu}(\text{NCS})_2$ obtained by ac susceptibility measurements. The superconducting transition temperature $T_c = 8.6$ K is defined by a 10% change of the signal.

The surface impedance is defined as

$$\hat{Z}_S = \frac{E_0}{\int_0^\infty j dx}, \quad (1)$$

where E_0 is the electric field at the surface, j is the ac current induced in the sample and the x direction is normal to the surface. \hat{Z}_S is, in terms of the complex conductivity $\hat{\sigma} = \sigma_1 + i\sigma_2$, given by

$$\hat{Z}_S = R_S + iX_S = \left(\frac{i\mu_0\omega}{\sigma_1 - i\sigma_2} \right)^{1/2}, \quad (2)$$

where R_S and X_S are the surface resistance and surface reactance, respectively. In the normal state, at frequencies $\omega\tau < 1$, the conductivity $\sigma_1 \ll \sigma_2$ and

$$R_S = X_S = \left(\frac{\mu_0\omega}{2\sigma_{dc}} \right)^{1/2}, \quad (3)$$

i.e., the surface resistance is equal to the surface reactance in the so-called Hagen Rubens limit, and $\sigma_1(\omega \ll 2\pi/\tau) \approx \sigma_{dc}$. Consequently, at low frequencies the resistivity is given by

$$\rho(T) = 2R_S^2/\mu_0\omega. \quad (4)$$

In Fig. 1 we display dc resistivity of $(\text{BEDT-TTF})_2\text{Cu}(\text{NCS})_2$ as a function of temperature together with the high frequency resistivity evaluated from microwave

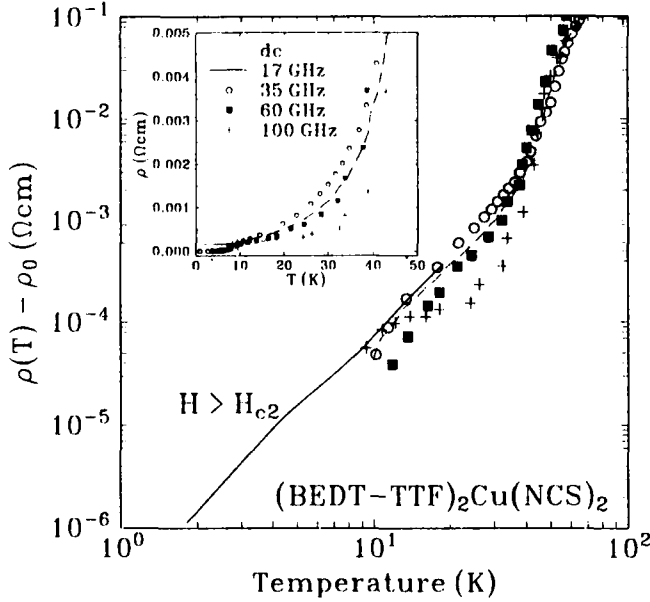


FIGURE 2: The temperature dependence of the resistivity $\rho(T) - \rho_0$ of $(\text{BEDT-TTF})_2\text{Cu}(\text{NCS})_2$ plotted in a double logarithmic way. The inset shows $\rho(T)$ on linear axes. The solid line represents the data taken by Achkir et al. [15] in the presence of a 9 Tesla magnetic field.

surface impedance measurements at 35 GHz, 60 GHz and 100 GHz [8] by using Eq. (4). The data are normalized at low temperatures with $\sigma_{dc}(T = 15 \text{ K}) = 3.8 \times 10^3 (\Omega\text{cm})^{-1}$. The superconducting transition is as high as 10.4 K for the resistivity midpoint and $T_c \approx 8.6 \text{ K}$ from ac-susceptibility measurements with a transition of more than 1 K wide as can be seen in the inset Fig. 1. The temperature dependence goes through a broad maximum at around 100 K which is not entirely understood yet. $\rho(T)$ drops sharply at lower temperatures indicating a metallic behavior. The same overall T -dependence is observed at all frequencies up to 100 GHz confirming the Hagen-Rubens assumption. Perpendicular to the highly conducting (bc)-plane, the conductivity is smaller by a factor of 1000 and at $T = 12 \text{ K}$ it reaches the absolute value of $\sigma_{\perp}(T = 15 \text{ K}) = 4 (\Omega\text{cm})^{-1}$. The temperature dependence, however, was found to be similar [8].

In the range below 30 K the resistivity shows a parabolic form which even extends for $T < 10 \text{ K}$ if the superconducting phase is suppressed by an external magnetic field $H \gg H_{c2}$ [15]. The inset of Fig. 2 displays the low temperature part of the $\rho(T)$ obtained at different frequencies; the 17 GHz data were measured by Achkir et al. [15] under a magnetic field of 9 Tesla. In Fig. 2 the resistivity $\rho(T)$ is plotted as a function of temperature in a double logarithmic way after subtracting the residual resistivity $\rho_0 \approx 150 \mu\Omega\text{cm}$ caused by impurity scattering. If phonon scattering is dominant, a T^5 behavior is expected at low temperatures; electron-electron scattering on the other hand leads to a T^2 behavior. As seen from Fig. 2, in a reasonably wide temperature range from 1.5 K up to 35 K, $\rho(T) - \rho_0$ observes

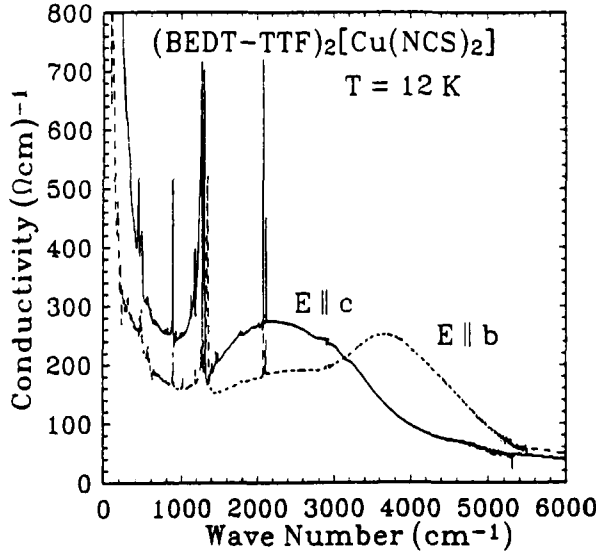


FIGURE 3: The optical conductivity $\sigma(\omega)$ of $(\text{BEDT-TTF})_2\text{Cu}(\text{NCS})_2$ for $\vec{E} \parallel b$ and $\vec{E} \parallel c$ as evaluated from reflectivity measurements at $T = 12$ K by KK analysis (after Kornelsen et al. [2]).

a power law close to T^2 :

$$\rho(T) = \rho_0 + AT^2 \quad (5)$$

with $A \approx 8 \times 10^{-7} \Omega\text{cm}/\text{K}^2$. This behavior is typical for an interacting electron gas, described by the Landau theory of a Fermi liquid [16, 17, 18]. The prefactor A increases with increasing electron-electron interaction. The relation $A \propto \gamma^2$, with γ the Sommerfeld coefficient obtained from specific heat, was confirmed for a large number of materials. While most narrow-band systems, like the heavy fermions but also Rb_3C_{60} , fall on a line with $A/\gamma^2 = 10^{-5}$ [19], $(\text{BEDT-TTF})_2\text{Cu}(\text{NCS})_2$ has a much larger ratio of about 10^{-3} , which may infer that the resistivity is dominated by phonons.

Extensive investigations of the optical properties of $\kappa\text{-(BEDT-TTF)}_2\text{Cu}(\text{NCS})_2$ single crystals have been conducted by John Eldridge's group [2, 3, 4]. The reflectivity in both directions of the conducting plane was measured at various temperatures in the frequency range from 200 cm^{-1} to 8000 cm^{-1} . As a result of the KK analysis the optical conductivity $\sigma_1(\omega)$ in the normal state ($T = 12 \text{ K}$) is displayed in Fig. 3. As expected from the roughly isotropic dc conductivity in the (bc) -plane, the overall optical properties are the same in both directions. Neither the high nor the low-temperature results follow a simple Drude behavior given by

$$\hat{\sigma}(\omega) = \sigma_1(\omega) + i\sigma_2(\omega) = \frac{\sigma_{dc}}{1 - i\omega\tau} = \frac{\omega_p^2}{4\pi} \frac{1}{1/\tau - i\omega}, \quad (6)$$

where the plasma frequency is defined as

$$\omega_p = \left(\frac{4\pi ne^2}{m_b} \right)^{1/2}, \quad (7)$$

with n the number of free charge carriers and m_b the band mass. The overall conductivity spectrum can be interpreted as a combination of a FIR contribution from intraband transitions (narrow peak at $\omega = 0$) and a MIR interband contribution (seen as a broad maximum around 2000 cm^{-1} to 4000 cm^{-1}). Ascribing only the narrow FIR peak ($\omega_p \approx 2600 \text{ cm}^{-1}$, $1/\tau \approx 40 \text{ cm}^{-1}$) to the quasi-free carriers, however, leads to an effective mass $m_b \approx 15m_e$ (where m_e is the free electron mass) which appears unreasonably large. A fit of the MIR range describes the $T = 12 \text{ K}$ reflectivity data sufficiently at frequencies above 3500 cm^{-1} (but ignores the FIR peak) and leads to $\omega_p = 8730 \text{ cm}^{-1}$, $1/\tau = 1260 \text{ cm}^{-1}$ and $\epsilon_\infty = 3.37$ in the b -direction, and to $\omega_p = 8520 \text{ cm}^{-1}$, $1/\tau = 1195 \text{ cm}^{-1}$ and $\epsilon_\infty = 4.13$ for $\vec{E} \parallel c$. From sum-rule arguments [20]

$$\int_0^\infty \sigma_1(\omega) d\omega = \frac{\pi n e^2}{2m_b} = \frac{\omega_p^2}{8}. \quad (8)$$

one can estimate $\omega_p = 7000 \text{ cm}^{-1}$ and 7500 cm^{-1} for $\vec{E} \parallel b$ and $\vec{E} \parallel c$, respectively [2]. Assuming a carrier density $n = 1.23 \times 10^{21} \text{ cm}^{-3}$ resulting from one charge per two BEDT-TTF molecules, the effective mass can then be calculated to $m_b = 2.4m_e$, which is in good agreement with the estimations from Shubnikov-de Haas and de Haas-van Alphen experiments [21, 22].

The Drude model which leads to Eq. (6) assumes a frequency independent scattering process and effective mass. In particular at low temperatures, this may not be adequate. Another method of analyzing the data is to consider free carriers which are scattered with a frequency dependent damping $1/\tau(\omega)$ so that the complex conductivity may be written as

$$\hat{\sigma}(\omega) = \frac{\omega_p^2/4\pi}{1/\tau(\omega) - i\omega m^*(\omega)/m_e}, \quad (9)$$

which is known as the generalized Drude formula. The relationship between $\sigma_1(\omega)$, $\sigma_2(\omega)$ and $1/\tau(\omega)$ together with $m^*(\omega)/m_e$ is then obtained as follows

$$\frac{1}{\tau(\omega)} = \frac{\omega_p^2 \sigma_1(\omega)}{4\pi |\hat{\sigma}(\omega)|^2} \quad (10)$$

and

$$\frac{m^*(\omega)}{m_e} = \frac{\omega_p^2 \sigma_2(\omega)/\omega}{4\pi |\hat{\sigma}(\omega)|^2} \quad (11)$$

When $\omega \ll 1/\tau$ and $\omega \rightarrow 0$, σ_1 becomes constant and σ_2 tends to zero, but $1/\tau(\omega, T)$ and $m^*(\omega, T)/m_e$ assume a constant value. In Fig. 4 the frequency dependence of the scattering rate $1/\tau(\omega)$ is plotted for $(\text{BEDT-TTF})_2\text{Cu}(\text{NCS})_2$ at about 12 K . In addition to the optical results [2], the estimations from microwave and millimeter wave cavity perturbation measurements [8] at 35 GHz and 60 GHz (cf. Tab. I) are shown, as well as result from Shubnikov-de Haas experiments [21] ($1/\tau = 2 \text{ cm}^{-1}$) at the left end of the frequency scale. A strong frequency dependence of $1/\tau$ is found, which does not simply follow a power law. For $\omega > 100 \text{ cm}^{-1}$, $1/\tau \propto \omega^2$ is approached; for lower frequencies, however, the scattering rate increases slower than linear with frequency.

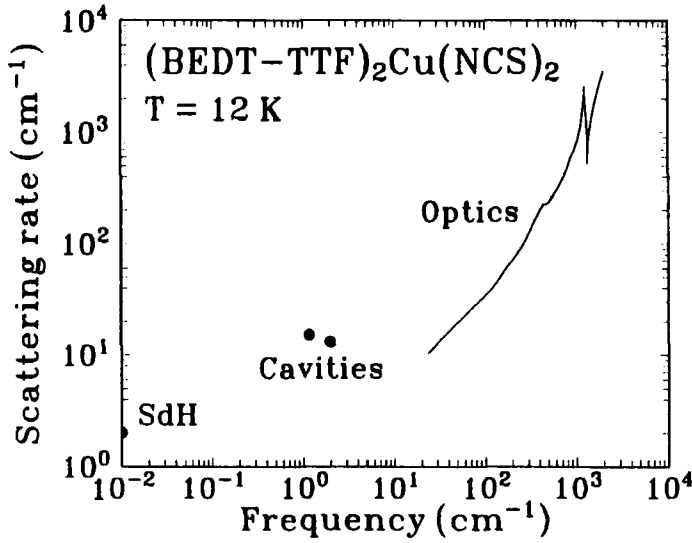


FIGURE 4: Frequency dependent scattering rate $1/\tau$ as obtained by a generalized Drude analysis of the optical data (taken from Kornelsen et al. [2]). Also shown are the results of Shubnikov-de Haas measurements [21] and the experiments performed in microwave cavities at 35 GHz and 60 GHz.

According to Landau's theory of a Fermi liquid, we would expect that [17, 23, 24]

$$\frac{1}{\tau(T, \omega)} \propto \left[(2\pi k_B T)^2 + (\hbar\omega)^2 \right], \quad (12)$$

i.e. the frequency dependence of the scattering rate follows the T^2 -dependence of the resistivity since $\rho \propto 1/\tau$. The proportionality factor depends on the renormalized bandwidth and the electron-electron scattering cross-section [23, 24]. It should be pointed out, however, that the ω^2 -dependence is only predicted if $\hbar\omega > k_B T$, which is not the case for the microwave measurements on $(\text{BEDT-TTF})_2\text{Cu}(\text{NCS})_2$. Further experiments at lower temperatures have to be carried out in the presence of a magnetic field $H > H_{c2}$ in order to suppress superconductivity.

SUPERCONDUCTING PROPERTIES

κ -(BEDT-TTF) $_2$ Cu(NCS) $_2$ undergoes a superconducting transition at about 10 K. Although the superconducting gap calculated by the standard BCS formula of the weak coupling limit $2\Delta = 3.53k_B T_c$ is expected at approximately 20 to 25 cm^{-1} , no indications of an energy gap could be seen in optical absorption measurement down to a frequency of 10 cm^{-1} and at $T \approx 5.1$ K [3]. As can be seen from Fig. 1, the surface resistance obtained by experiments in the millimeter wave range up to 3 cm^{-1} drops upon entering the superconducting phase.

For a BCS superconductor in the dirty limit, the electrodynamic response has been evaluated first by Mattis and Bardeen [25]:

$$\frac{\sigma_{1,s}(\omega, T)}{\sigma_n} = \frac{2}{\hbar\omega} \int_{\Delta}^{\infty} [f(E) - f(E + \hbar\omega)] g(E) dE$$

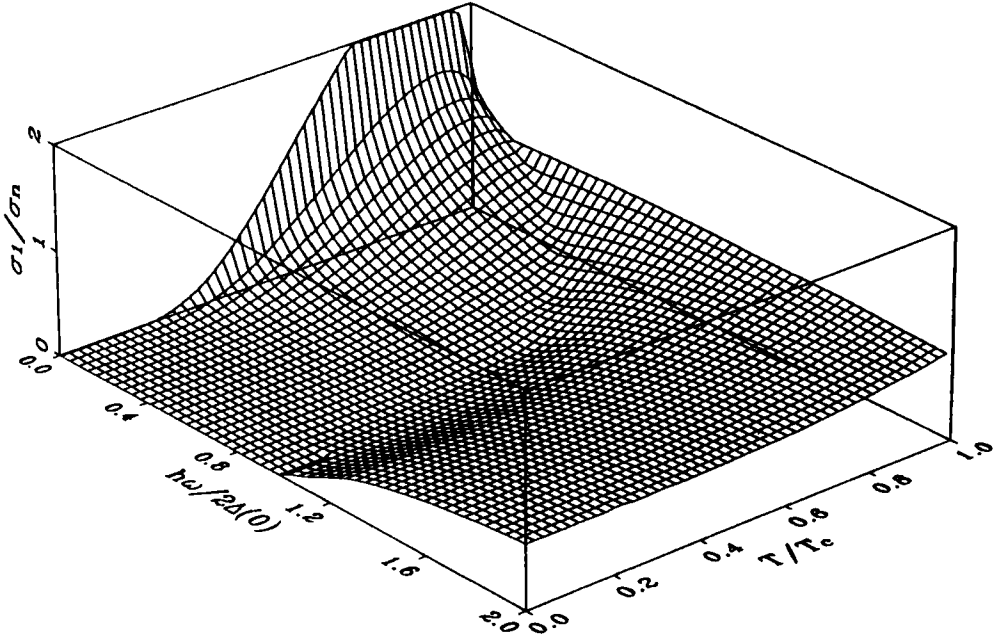


FIGURE 5: The real part of the normalized conductivity σ_1/σ_n of a superconductor as a function of frequency $\hbar\omega/2\Delta$ and temperature T/T_c calculated after Eq. (13) derived by Mattis and Bardeen [25].

$$+ \frac{1}{\hbar\omega} \int_{\Delta-\hbar\omega}^{-\Delta} [1 - 2f(E + \hbar\omega)]g(E)dE \quad (13)$$

$$\frac{\sigma_{2,s}(\omega, T)}{\sigma_n} = \frac{1}{\hbar\omega} \int_{\Delta-\hbar\omega, -\Delta}^{\Delta} \frac{[1 - 2f(E + \hbar\omega)](E^2 + \Delta^2 + \hbar\omega E)}{(\Delta^2 - E^2)^{1/2}[(E + \hbar\omega)^2 - \Delta^2]^{1/2}} dE, \quad (14)$$

where

$$f(E) = \frac{1}{e^{E/k_B T} + 1}$$

$$g(E) = \frac{(E^2 + \Delta^2 + \hbar\omega E)}{(E^2 - \Delta^2)^{1/2}[(E + \hbar\omega)^2 - \Delta^2]^{1/2}},$$

and the limits of integration are those specified in the original paper. The only input parameters in these calculations are the values of the energy gap Δ (which is determined by the transition temperature T_c), the temperature T , and the frequency ω . In Fig. 5 the real part of the conductivity $\sigma_1(\omega)/\sigma_n$ is plotted as a function of temperature T/T_c and frequency $\hbar\omega/2\Delta$. At low temperatures $\sigma_1(\omega)/\sigma_n$ drops to zero below the superconducting gap energy which leads to a vanishing absorption. For temperatures slightly below the transition temperature T_c , a maximum of the conductivity is expected at low frequencies, known as the coherence peak [26]. The height of the peak goes as:

$$\left(\frac{\sigma_1}{\sigma_n}\right)_{\max} \propto \log \left\{ \frac{2\Delta(0)}{\hbar\omega} \right\} \quad (15)$$

The peak only appears for $\hbar\omega \leq \Delta/5$ (well below 2Δ); the width of the peak is only slightly frequency dependent as seen in Fig. 5. $\sigma_1(T)/\sigma_n$ can be approximated by the following algebraic formula:

$$\frac{\sigma_1(T)}{\sigma_n} \approx 2f[\Delta(T)] \left[1 + \frac{\Delta(T)}{k_B T} [1 - f(\Delta(T))] \ln \left\{ \frac{2\Delta(T)}{\hbar\omega} \right\} \right]. \quad (16)$$

On the other hand, in the dirty limit ($\ell < \xi_0$) the imaginary part of the conductivity σ_2/σ_n is related to the gap parameter through the expression [26]:

$$\frac{\sigma_2(\omega, T)}{\sigma_n} = \frac{\pi \Delta(T)}{\hbar\omega} \tanh \left[\frac{\Delta(T)}{2k_B T} \right] \approx \lim_{T \rightarrow 0} \frac{\pi \Delta(T=0)}{\hbar\omega}. \quad (17)$$

In the clean limit ($\ell > \xi_0$), however, σ_2/σ_n tends to the ratio $1/\omega\tau$ at low temperatures, and so in our case we cannot extract Δ from the zero-temperature value of σ_2 , though we can check the consistency as far as the crossover from the Hagen-Rubens regime ($\omega\tau < 1$) to the relaxation regime ($\omega\tau > 1$) is concerned.

In order to investigate the surface impedance of $(\text{BEDT-TTF})_2\text{Cu}(\text{NCS})_2$ for $T < T_c$, have been employed two enclosed cavity configurations, one at 35 GHz and one at 60 GHz [12, 13, 14]. The experiments were performed with the electric \vec{E}_{ac} parallel to the c -direction, and consequently $\hat{Z}_{S\parallel}$ is probed. The complex conductivity $\hat{\sigma} = \sigma_1 + i\sigma_2$ in the superconducting state which can be evaluated from both $R_S(T)$ and $X_S(T)$ by using Equation 2:

$$\sigma_1 = \frac{2\omega R_S X_S}{(R_S^2 + X_S^2)^2} \quad \text{and} \quad \sigma_2 = \frac{\omega(X_S^2 - R_S^2)}{(R_S^2 + X_S^2)^2}. \quad (18)$$

The temperature dependence of the real and imaginary part of the normalized conductivity σ_1/σ_n and σ_2/σ_n is shown in Fig. 6. The measurements at 35 GHz and 60 GHz were performed at two different crystals with slightly different transition temperature ($T_c = 8.6$ K and 8.3 K, respectively). In order to normalize the conductivity to the metallic state value, we assume a temperature dependent scattering rate yielded from a fit of the metallic resistivity above T_c given by Eq. (5), and extrapolate this behavior below the transition as justified by Fig. 2. The general outcome of both experiments is similar: σ_2 rises rapidly for $T < T_c$ and basically follows the temperature dependence of the superconducting energy gap [Eq. (17)]. The real part of the conductivity σ_1 shows a maximum just below T_c which is stronger developed at lower frequencies.

Both of our results shown in Fig. 6 are in full agreement with a BCS ground state. The small coherence peak in the σ_1 -curve finds a natural explanation in the BCS model: the broad maximum reflects the case-II coherence factor [26]. At 60 GHz the photon energy is comparable to the single particle gap Δ , and the peak is almost smeared out. The experiments at 35 GHz exhibit a peak value of $\sigma_1/\sigma_n \approx 1.35$, again in the excellent agreement with the BCS theory. We note that higher-momentum pairing leads to the rapid disappearance of the coherence peak and is expected to give $\sigma_1(T)$ values significantly below the solid line in Fig. 6. The size of the coherence peak depends on the coherence factor plus the divergency of the excitation density of states at the the gap edge. It is expected that this singularity is removed for

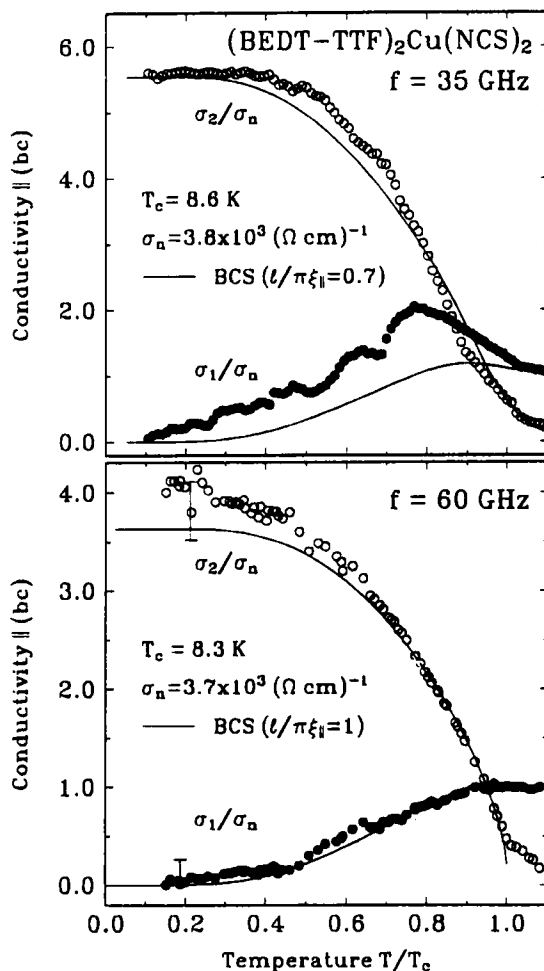


FIGURE 6: Temperature dependence of both components of the optical conductivity σ_1 and σ_2 of κ -(BEDT-TTF) $_2$ Cu(NCS) $_2$ normalized to the normal state conductivity σ_n . The measurements were performed at 35 GHz and 60 GHz with the electric field parallel to the highly conducting layers. The solid lines represent the results of the BCS theory with $\ell/\pi\xi_l = 0.7$ and 1, respectively.

TABLE I: Electrodynamical properties of $(\text{BEDT-TTF})_2\text{Cu}(\text{NCS})_2$ with the current flowing parallel to the highly conducting (bc)-plane; one crystals was measured at 35 GHz, the second at 60 GHz. The coherence length was assumed to be 70 \AA , the superconducting energy gap was estimated by $2\Delta = 3.53k_B T_c \approx 21 \text{ cm}^{-1}$. δ_0 is the skin depth evaluated at $T = 9 \text{ K}$, ℓ the mean free path, $1/\tau$ the scattering rate, and λ the zero temperature penetration depth.

$\omega/2\pi$ (GHz)	T_c (K)	$\sigma_1(T = 15 \text{ K})$ ($\Omega^{-1}\text{cm}^{-1}$)	δ_0 (μm)	ℓ (\AA)	$1/\tau$ (cm^{-1})	$\lambda(T = 0)$ (μm)
35	8.6	3.8×10^3	4.4	160	15	0.8
60	8.3	3.7×10^3	3.4	220	13	1.4

d-wave pairing leading to a sharp decrease of the optical conductivity analogous to the Yosida function.

The dirty limit ($\ell < \xi_0$) assumed in the derivation of Eqs. (13) and (14) may not be appropriate for κ -(BEDT-TTF)₂Cu(NCS)₂, since the mean free path $l \approx 100$ Å is comparable to the coherence length $\xi_0 = 70$ Å [27]. Chang and Scalapino [28] went beyond the treatment of Mattis and Bardeen, assuming a two-dimensional BCS ground state. We restricted ourselves to the weak coupling limit $\Delta(T = 0\text{K}) = 1.76k_B T_c$ and fitted our results for various values of the only remaining parameter $\ell/\pi\xi_0$. The best fits of our 35 and 60-GHz data shown in Fig. 6 led to a value of $\ell/\pi\xi = 0.7$ and 1.0, respectively. Using with $v_F = 4.7 \times 10^6$ cm/s, the scattering rate $1/\tau$ was estimated and listed in Tab. I.

In the superconducting state well below T_c the surface reactance is given by

$$X_S(T) = \mu_0 \omega \lambda(T), \quad (19)$$

where the surface reactance $X_S(T)$, which is proportional to the measured frequency shift, is proportional to the penetration depth λ and therefore can be directly compared with various models of the superconducting state.

The experimental results were obtained using the 35 GHz cavity which can be cooled down with ³He to $T \approx 0.7$ K. The measured penetration depth of (BEDT-TTF)₂Cu(NCS)₂ in the two directions is displayed in Fig. 7 in comparison with theoretical predictions of the weak coupling BCS theory. Within our accuracy of $\delta\lambda/\lambda = \pm 0.007$ [14], no indication of a temperature dependence can be found below 0.3 T_c . The absolute value of the zero temperature penetration depth $\lambda(T = 0) = 0.8$ μm was found in good agreement with the literature values of 0.78 μm and 0.98 μm as obtained by μ SR [29, 30]. The analysis of our 60 GHz data in leads to $\lambda(T = 0) = 1.4$ μm. We note that in contrast to the temperature dependence, the determination of the absolute value of the penetration depth requires an accurate knowledge of the sample geometry and of a temperature independent frequency offset introduced upon opening the cavity [13, 14]; this leads to an uncertainty in the absolute value of λ but does not influence $\lambda(T)/\lambda(0)$. The dotted line in Fig. 7 is the London limit ($\lambda > \ell > \xi_0$), the dashed line represents the local regime ($\lambda > \xi_0 > \ell$), and the solid line was calculated using the two-fluid model

$$\lambda_T(T) = \lambda_0 [1 - (T/T_c)^4]^{-1/2} \quad (20)$$

which is close to $\lambda(T)$ as would be observed for strong coupling. From our penetration depth data we cannot distinguish between clean ($\ell > \xi_0$) and the dirty limit ($\xi_0 > \ell$).

For a finite mean free path $\ell = 150$ Å the measured penetration depth λ exceeds the London penetration depth λ_L :

$$\lambda(T = 0) = \lambda_L(T = 0) \left(1 + \frac{\xi_0}{\ell} \right)^{1/2}, \quad (21)$$

where $\xi_0 = 70$ Å is the coherence length. Using Pippard's formula

$$\frac{1}{\lambda_L^2} = \frac{8}{c^2} \int \sigma_1 d\omega = \left(\frac{\omega_p}{c} \right)^2, \quad (22)$$

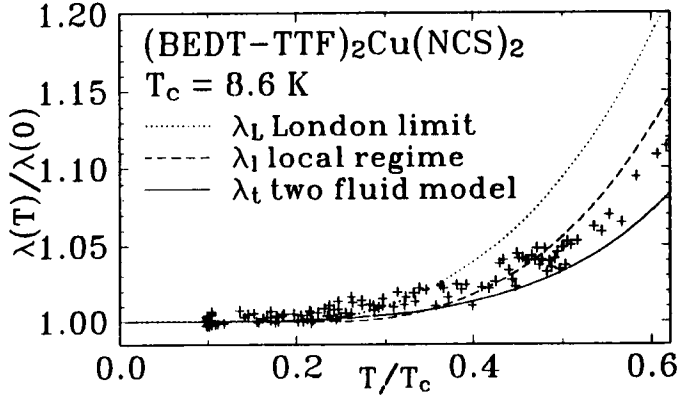


FIGURE 7: The penetration depth in $(\text{BEDT-TTF})_2\text{Cu}(\text{NCS})_2$ as a function of temperature compared with theoretical predictions. The dotted line is the BCS weak coupling limit, the dashed line represents the local regime, and the full line is the two fluid model. In agreement with the calculations there is no appreciable temperature dependence below $0.3 T_c$.

where the plasma frequency ω_p is given by Eq. (7). λ_L can be estimated from the normal state parameters

$$\lambda_L(T=0) = \left(\frac{m^*}{\mu_0 e^2 n} \right)^{1/2}. \quad (23)$$

From this we obtain $\lambda_L(T=0) = 0.79 \mu\text{m}$ and consequently $\lambda(T=0) = 0.95 \mu\text{m}$, which agrees well with our experimental data.

The temperature dependence of the penetration depth is a direct indication of the pairing mechanism. Since $\lambda(T)$ is governed by the quasi-particle excitation spectrum, zeros of the order parameter should result in an anisotropic and power-law T -dependence of $\lambda(T \rightarrow 0)$ due to the enhanced pair breaking excitations at low temperatures. While d -wave pairing results in a linear temperature dependence [31], s -wave pairing leads to a flat behavior with $d\lambda(T)/dT|_{T \rightarrow 0} = 0$. It is clear from Fig. 7, that $\lambda(T)$ is well described by assuming a conventional s -wave ground state.

CONCLUSION

In the temperature region above T_c (but $T < 100 \text{ K}$) κ -(BEDT-TTF) $_2$ Cu(NCS) $_2$ behaves like metals with a scattering rate of approximately 15 cm^{-1} . The electrodynamic properties cannot be satisfactorily described by the simple Drude model where a frequency independent scattering time is assumed [Eq. (6)]. The T^2 dependence of the resistivity for $T < 30 \text{ K}$ and the results of a generalized Drude analysis indicate that electron-electron interaction cannot be neglected in these organic materials. Further studies are required to fully clarify the normal state properties in this regard.

The electrodynamic properties of $(\text{BEDT-TTF})_2\text{Cu}(\text{NCS})_2$ in the superconducting phase can be well described by the BCS theory assuming a conventional s -wave pairing. The coherence peak in σ_1 below T_c follows the predicted frequency dependence and rules out a superconducting ground state which is significantly different

from singlet pairing. The penetration depth $\lambda(T)$ of the organic superconductors κ -(BEDT-TTF)₂Cu(NCS)₂ shows a flat behavior for low temperatures. This is in agreement with the BCS prediction and conventional *s*-wave pairing.

Similar investigations in the optical [32] and microwave and millimeter wave [8] range have been performed on (BEDT-TTF)₂Cu[N(CN)₂]Br and lead to comparable results. Thus we can conclude that the discussed behavior is general for class of two dimensional organic superconductors. Nevertheless, it will be desirable to revisit these issues when samples with extremely sharp superconducting transitions become available.

Acknowledgements In the course of this work, we enjoyed the collaboration and discussions with J.E. Eldridge, O. Klein, and K. Kornelsen. The (BEDT-TTF)₂-Cu(NCS)₂ crystals used in this study were grown by the group of J.M. Williams at Argonne National Laboratory.

REFERENCES

- [1] C.S.Jacobsen, D.B. Tanner, and K. Bechgaard, Phys. Rev. Lett. **46**, 1142 (1981); Mol. Crys. Liq. Cryst. **79**, 25 (1982); Phys. Rev. B **28**, 7019 (1983).
- [2] K. Kornelsen, J.E. Eldridge, C.C. Homes, H.H. Wang and J.M. Williams, Solid State Commun. **72**, 475 (1989).
- [3] K. Kornelsen, J.E. Eldridge, H.H. Wang and J.M. Williams, Solid State Commun. **76**, 1009 (1990).
- [4] K. Kornelsen, J.E. Eldridge, H.H. Wang and J.M. Williams, Phys. Rev. B **44**, 5235 (1991).
- [5] K. Holczer, D. Quinlivan, O. Klein, G. Grüner, and F. Wudl, Solid State Commun. **76**, 499 (1990); K. Holczer, O. Klein, G. Grüner, H. Yamochi, and F. Wudl, in Organic Superconductivity, ed. by V.Z. Kresin and W.A. Little, (Plenum Press, New York, 1990).
- [6] O. Klein, K. Holczer, G. Grüner, J.J. Chang, and F. Wudl, Phys. Rev. Lett. **66**, 655 (1991).
- [7] M. Dressel, S. Bruder, G. Grüner, K.D. Calson, H.H. Wang, and J.M. Williams, Phys. Rev. B **48**, 9906 (1993).
- [8] M. Dressel, O. Klein, G. Grüner, K.D. Calson, H.H. Wang, and J.M. Williams, Phys. Rev. B **50**, 13603 (1994).
- [9] J.M. Williams, J.R. Ferraro, R.J. Thorn, K.D. Carlson, U. Geiser, H.H. Wang, A.M. Kini, and M.-H. Whangbo, Organic Superconductors (Prentice Hall, Englewood Cliffs NJ, 1992).
- [10] H. Urayama, H. Yamochi, G. Saito, K. Nozawa, T. Sugano, M. Kinoshita, S. Sato, K. Oshima, A. Kawamoto, and J. Tanaka, Chem. Lett. **55**, 1988 (1988).
- [11] L.I. Buravov, A.V. Zvarykina, N.D. Kushch, V.N. Laukhin, V.A. Merzhanov, A.G. Khomenko, and E.B. Yagubskii, Sov. Phys. JETP, **68**, 182 (1989).
- [12] O. Klein, S. Donovan, M. Dressel, and G. Grüner, Int. J. Infrared Millimeter Waves **14**, 2423 (1993).
- [13] S. Donovan, O. Klein, M. Dressel, K. Holczer, and G. Grüner, Int. J. Infrared Millimeter Waves **14**, 2459 (1993).
- [14] M. Dressel, O. Klein, S. Donovan, and G. Grüner, Int. J. Infrared Millimeter Waves **14**, 2489 (1993).
- [15] D. Achkir, M. Poirier, C. Bourbonnais, G. Quirion, C. Lenior, P. Batail, and D. Jerome, Phys. Rev. B, **47**, 11595 (1993).
- [16] N.W. Ashcroft and N.D. Mermin, Solid State Physics, (Saunders College, Philadelphia, 1976).

- [17] A.A. Abrikosov, L.P. Gor'kov, and I.E. Dzyaloshinski, Methods of Quantum Field Theory in Statistical Physics (Prentice-Hall, Englewood, 1963).
- [18] P.S. Riseborough, Phys. Rev. B **27**, 5775 (1983).
- [19] T.T.M. Palstra, A.F. Hebard, R.C. Haddon, and P.B. Littlewood, Phys. Rev. B **50**, 3462 (1994).
- [20] F. Wooten, Optical Properties of Solids (Academic Press, San Diego, 1972).
- [21] N. Toyota, T. Sasaki, K. Murata, Y. Honda, M. Tokumoto, H. Bando, N. Kinoshita, H. Anzai, T. Ishiguro, and Y. Muto, J. Phys. Soc. Jpn. **57**, 2616 (1988).
- [22] K. Oshima, H. Urayama, H. Yamochi, and G. Saito, J. Phys. Soc. Japan **57**, 730 (1988); K. Oshima, Synth. Met. **27**, A419 (1988).
- [23] R.N. Gurzhi, Sov. Phys. JETP **35**, 673 (1959).
- [24] J. Ruvalds and A. Virosztek, Phys. Rev. B **43**, 5498 (1991).
- [25] D.C. Mattis and J. Bardeen, Phys. Rev. **111**, 412 (1958).
- [26] M. Tinkham, Introduction to Superconductivity (McGraw-Hill, New York, 1975).
- [27] G. Saito, Physica C **162-164**, 577 (1989).
- [28] J.J. Chang and D.J. Scalapino, Phys. Rev. B **40**, 4299 (1989).
- [29] D.R. Harshman, R.N. Kleiman, R.C. Haddon, S.V. Chichester-Hicks, M.L. Kaplan, L.W. Rupp, T. Pfiz, D.L. Williams, and D.B. Mitzi, Phys. Rev. Lett. **64**, 1293 (1990).
- [30] Y.J. Uemura, L.P. Le, G.M. Luke, B.J. Sternlieb, W.D. Wu, J.H. Brewer, T.M. Riseman, C.E. Stronach, G. Saito, H. Yamochi, H.H. Wang, A.M. Kini, K.D. Carlson, and J.M. Williams, in: Organic Superconductivity, edited by V.Z. Kresin and W.A. Little, (Plenum Press, New York, 1990).
- [31] F. Gross, B. S. Chandrasekhar, D. Einzel, K. Andres, P. J. Hirschfeld, H. R. Ott, J. Beuers, Z. Fisk, and J.L. Smith, Z. Physik B **64**, 175 (1986).
- [32] J. Eldridge, K. Kornelsen, H. Wang, J. Williams, A.D. Crouch, and D. Watkins, Solid State Commun. **79**, 583 (1991).